The Astrophysical Journal, 634:70–76, 2005 November 20

THE COMPRESSION OF DARK MATTER HALOS BY BARYONIC INFALL

J. A. Sellwood
Department of Physics and Astronomy, Rutgers University, 136 Frelinghuysen Road, Piscataway, NJ 08854-8019; sellwood@physics.rutgers.edu

and

Stacy S. McGaugh
Department of Astronomy, University of Maryland, College Park, MD 20742-2421; ssm@astro.umd.edu
Received 2005 June 20; accepted 2005 July 29

ABSTRACT

The initial radial density profiles of dark matter halos are laid down by gravitational collapse in hierarchical structure formation scenarios and are subject to further compression as baryons cool and settle to the halo centers. Here we describe an explicit implementation of the algorithm, originally developed by Young, to calculate changes to the density profile as the result of adiabatic infall in a spherical halo model. Halos with random motion are more resistant to compression than are those in which random motions are neglected, which is a key weakness of the simple method widely employed. Young's algorithm results in density profiles in excellent agreement with those from *N*-body simulations. We show how the algorithm can be applied to determine the original uncompressed halos of real galaxies, a step that must be computed with care in order to enable a confrontation with theoretical predictions from theories such as ΛCDM.

Subject headings: dark matter — galaxies: formation — galaxies: halos — galaxies: kinematics and dynamics

1. INTRODUCTION

Initial density fluctuations in the early universe are widely believed to seed the collapse of dark matter halos through gravitational instability. Computation of this process has allowed the clustering and properties of the collapsed halos to be predicted in detail in simulations of the collisionless component only (e.g., Navarro et al. 1997, 2004; Jing 2000; Bullock et al. 2001; Diemand et al. 2004).

Initially, the dark matter and hot gas are well mixed (Spergel et al. 2003), but galaxies are believed to form as the baryons cool and settle toward the centers of collapsed halos, as originally envisaged by White & Rees (1978), Fall & Efstathiou (1980), Gunn (1982), and others. The settling of gas toward the center causes further compression of the halo. This latter process is followed directly in simulations that include gas cooling (Gottlöber et al. 2003; Abadi et al. 2003; Governato et al. 2004), but an approximate analytic treatment is needed for many applications. The conventional procedure (Blumenthal et al. 1986) is widely used to compute, for example, the expected surface brightness (e.g., Dalcanton et al. 1997; Mo et al. 1998), more elaborate semi-analytic galaxy formation models (e.g., Cole et al. 2000; van den Bosch & Dalcanton 2000), predictions for lensing (e.g., Keeton 2001), and predictions from tilted power spectra (e.g., Zentner & Bullock 2002). It has been reported that the Blumenthal formula generally overestimates the actual compression (Barnes 1987; Sellwood 1999; Gnedin et al. 2004).

However, Young (1980) showed that adiabatic compression of a spherical system can be treated exactly, without having to run expensive simulations. His formulation was originally devised to model the growth of a black hole in a spherical star cluster, but the method can be applied for any adiabatic change to a spherical potential. It was first used for halo compression by Wilson (2004) and developed independently by us.

We review the standard method for halo compression in § 2 and describe Young's (1980) method in § 3. We give a few examples and tests in § 4 and illustrate the application of the method to data from real galaxies in § 5.

2. HALO COMPRESSION

The usual algorithm for halo compression is easy to implement but very crude. It is generally attributed to Blumenthal et al. (1986), although the same idea was developed independently by Barnes & White (1984), Ryden & Gunn (1987), and others. It assumes that dark matter particles conserve only their angular momenta as the halo is compressed, which is equivalent to assuming that all the halo particles move on circular orbits (see below). In a spherical potential, the squared angular momentum of a circular orbit is $L^2 = rGM(r)$, and if this quantity is conserved as a disk with the mass profile $M_d(r)$ grows slowly, we have

$$r_i M_i(r_i) = r_f \left[M_d\left(r_f\right) + (1 - f_d) M_f\left(r_f\right) \right], \tag{1}$$

where M_i is the initial total mass (dark plus baryonic) profile, $(1 - f_d)M_f$ is the desired final dark matter mass profile, and r_f is the final radius of the mass shell initially at radius r_i. The quantity f_d is the fraction of the initial total mass, assumed to be independent of radius, that condenses to form the disk. We can substitute for $M_f(r_f)$ by making use of the assumption

$$M_i(r_i) = M_f\left(r_f\right), \tag{2}$$

which is sometimes stated as "shells of matter do not cross." We can then find r_i for any desired r_f, and through equation (2), we can obtain the mass profile of the compressed dark matter halo. For convenience, we denote this the Blumenthal algorithm.

Equation (1) assumes that the disk mass is taken from the halo in equal proportions at all radii. A possible alternative assumption is to imagine that the mass of the disk arrives from an external source, in which case the right-hand side reads $r_f[M_d(r_f) + M_f(r_f)]$. Scaling the compressed mass profile by the factor $1/(1 + f_d)$

would conserve total mass once more and result in a scaled density profile that is not mathematically identical to that resulting from the more common procedure, but differences are small everywhere. Neither hypothesis is likely to be correct, since the condensing mass fraction depends on factors such as the cooling rate at each radius, but such refinements are unlikely to affect the inner halo density much.

Flores et al. (1993) report some *N*-body tests that indicated that the Blumenthal algorithm yields a reasonable approximation to the compressed halo, and Jesseit et al. (2002) reached a similar conclusion. But Barnes (1987), Sellwood (1999), and Gnedin et al. (2004) have warned that the predicted density profile is more concentrated than that found in their *N*-body simulations, especially in the crucial inner part. Gnedin et al. suggest that the above scheme be amended to take into account the radial motions of the particles and recommend the substitution $M(r)r \rightarrow M(\bar{r})r$ in equation (2), where $\bar{r}$ is the time-averaged radius of each halo particle. Their revised formula gives better agreement with their simulations, in which halos are not perfectly relaxed, but reduces to the Blumenthal prescription for equilibrium distribution functions of spherical halos.

A number of authors have reported difficulties when trying to apply the Blumenthal method to compute an original halo from the observed compressed form (e.g., Weiner et al. 2001). As long as the adiabatic assumption holds, valid formulae for compression can be employed to deduce the decompressed density. However, Weiner et al. found that the Blumenthal algorithm fails for decompression because the radial density profile can become multivalued, which is both physically impossible and inconsistent with the central assumption that "mass shells do not cross." Valid formulae for adiabatic changes must apply irrespective of the direction in which the change occurs, and the failure of the Blumenthal scheme in this regard is further evidence of its inadequacy.

3. YOUNG'S METHOD

As stressed in § 3.6 of Binney & Tremaine (1987, hereafter BT87), adiabatic changes conserve all three actions of an orbit. In a spherical system, the actions are the angular momentum and radial action, while the third action is identically zero because the plane of each orbit is an invariant. Thus, adiabatic compression of a spherical halo needs to take into account the conservation of radial action, as well as the angular momentum. (By ignoring the radial action, the Blumenthal algorithm implicitly assumes it is zero, and all particles move on circular orbits, as is well known.) Young (1980) described an algorithm that properly accounts for the effects of random motion in the halo while still assuming spherical symmetry, and similar considerations underlie the Fokker-Planck calculations of globular cluster evolution (e.g., Cohn 1979). Wilson (2004) has already applied the scheme we outline here for halo compression.

The assumption of spherical symmetry is crucial, since without it we would need to consider three actions, which would make the problem essentially intractable analytically, although it could still be followed in *N*-body simulations. Jesseit et al. (2002) and Wilson (2004) tested this assumption using *N*-body simulations, and we report an additional test in § 4 that indeed shows that the spherically averaged density profile agrees extremely well at all radii with the predicted change from a Young-type code. The effectiveness of the spherical assumption results from the fact that even quite heavy disks lead to very mild flattening of an isotropic halo, which justifies neglect of the third action.

The central idea of Young's method is to apply the constraint that the value of the distribution function (DF) expressed as a function of the actions is invariant during adiabatic changes; i.e., $f_0(J_r,\ J_\phi) = f_n(J_r,\ J_\phi)$. In this formula, $J_r(E, L)$ is the radial action, and $J_\phi \equiv L$ is the azimuthal action, or total angular momentum per unit mass, and the subscripts 0 and n refer to the original and new halo profiles, respectively. While f expressed as a function of the actions does not change, $f_n(E_n, L)$ does change because the relation between the radial action, J_r, and the specific energy, E_n, depends on the potential well.

Starting from some spherical initial model with density $\rho_0(r)$, potential $\Phi_0(r)$, and DF $f_0(E_0, L)$, we add a second mass component and search iteratively for new functions $\rho_n(r)$, $\Phi_n(r)$, and $f_n(E_n, L)$. At the nth iteration, we determine a new spherical density profile from

$$\rho_{n+1}(r) = 4\pi \int_{\Phi_n(r)}^{\Phi_n(\infty)} \int_0^{L_{\max}} \frac{L f_n(E_n,\ L)}{r^2 u}\, dL\, dE_n, \qquad (3)$$

where the radial speed

$$u = \left\{2[E_n - \Phi_n(r)] - L^2/r^2\right\}^{1/2}, \qquad (4)$$

and $L_{\max}(E) = r\{2[E - \Phi_n(r)]\}^{1/2}$. Since the value of f_n to be used in the integrand is determined by the condition $f_n(J_r,\ J_\phi) = f_0(J_r,\ J_\phi)$, we need to know $J_r(E_n,\ L)$ in the nth potential well and then to look up $E_0(J_r,\ L)$ in the initial potential well $\Phi_0(r)$, in order to evaluate $f_0(E_0,\ L)$. As these functions are not available in closed form, except for special potentials such as the isochrone (Eggen et al. 1962), we determine both by interpolation in two-dimensional tables of values; the table for $J_r(E_n,\ L)$ has to be updated at every iteration.

Since $\rho_{n+1}(r)$ is spherically symmetric, we have for halo compression

$$\Phi_{n+1}(r) = -G \int_r^\infty \frac{M_{n+1}(r')}{r'^2}\, dr' + \Phi_{\rm ext}(r). \qquad (5)$$

Note that $\Phi_{n+1}(r)$ includes $\Phi_{\rm ext}$, the monopole term only arising from the disk mass distribution. It is most convenient to create, and keep updated, one-dimensional tables for both $\Phi_n(r)$ and $\rho_n(r)$.

This new estimate of the gravitational potential is then used in equation (3) to obtain an improved estimate of the halo density, and the whole procedure is iterated until the solution converges. In practice, between 10 and 20 iterations are needed for the potential profile to stabilize to a part in 10^5. The method conserves mass; the final mass of compressed halo differs from the initial by a few parts in 10^4 for the grids we typically employ.

The disk mass can easily be subtracted from the halo if desired. All that is needed is to normalize the density given by equation (3) by the factor $(M_h - M_d)/M_h$. Here M_h is the mass of the halo to the virial radius. Alternatively, as we described above for the Blumenthal algorithm, one can renormalize the combined disk and halo masses to equal the original total mass.

This algorithm is clearly more difficult to program, and more time-consuming to run, than the Blumenthal algorithm. We use tables for ρ_n, Φ_n, etc. that typically have 100 radial points. The table for $J_r(E_n,\ L)$, which has to be rebuilt at every iteration, has 100×50 values, which, when fitted with a bicubic spline achieves interpolated estimates good to a part in 10^7 or better; constructing this table takes the lion's share of the computational effort. Nevertheless, the whole iterative scheme converges within a few CPU minutes.

Young (1980) showed that a given mass profile is less compressed when an isotropic DF is assumed than when all particles

have circular orbits, which is the implicit assumption of the Blumenthal algorithm. Thus, allowance for radial motion makes a dark matter halo somewhat more resistant to compression.

It should also be noted that even if the initial DF were isotropic, the compressed DF will not be. Since the DF of the compressed halo is computed anyway, Young's algorithm yields direct estimates of the radial anisotropy expected.

The method can, in principle, be adapted for halo decompression. Provided an equilibrium DF for the compressed halo can be constructed, the algorithm guarantees that the decompressed halo must have a positive, single-valued density everywhere. The only significant barrier to extending the method to this application is the construction from observational data of suitable DFs for compressed halos containing disks.

Young's method is not restricted to any particular radial mass profile for either the disk or the halo; the added external mass can have any spherically averaged mass profile. Nor is the method restricted to isotropic DFs; any $f(E,\ L)$ that yields the initial spherical mass profile may be used.

4. EXAMPLES AND TESTS

Figure 1 presents results from an N-body simulation designed to test the adequacy of the spherical approximation for the disk potential. This test uses the NFW density profile (Navarro et al. 1997)

$$\rho_N(r) = \frac{\rho_s r_s^3}{r(r+r_s)^2}, \tag{6}$$

with ρ_s setting the density scale at the break radius, r_s. We define a mass unit as $M_N = 4\pi\rho_s r_s^3$, which is equal to the mass enclosed within $r \simeq 5.3054 r_s$. The radial mass profile of an exponential disk is

$$m(R) = M_d\left[1-\left(1+\frac{R}{R_d}\right)\exp\left(-\frac{R}{R_d}\right)\right], \tag{7}$$

where M_d is the total mass of the disk and R_d is the disk scale length. We characterize a simple disk-halo model by two parameters: the mass ratio $m_d \equiv M_d/M_N$ and length ratio $l_d \equiv R_d/r_s$.

The isotropic DF for an NFW halo is given by Eddington's inversion formula (see § 4.4 of BT87) and is positive everywhere. This equation has to be solved numerically for the NFW potential, which requires a sophisticated quadrature method. It is convenient to impose an upper energy cutoff so that the halo density declines to zero at a large radius, but the boundary term should not be included. Alternatively, one can use Widrow's (2000) fitted approximation for the DF.

The halo is represented by 1 million particles selected smoothly from the DF, as described in Appendix B of Debattista & Sellwood (2000); in order to reduce shot noise when estimating the density in the inner halo, the halo particle masses were scaled as $\sqrt{L}$, where L is the total angular momentum of the particle. The disk in the simulation is represented by 100,000 equal mass particles that are added at a constant rate in the $z = 0$ plane and held fixed in their initial positions so that the disk mass profile remains exactly exponential. The halo particles move in response to forces from both the disk and halo, which are computed on a spherical grid of 500 radial shells (McGlynn 1984; Appendix A of Sellwood 2003) and include all multipole terms $0 \le \ell \le 8$. The disk is grown over the period $0 \le t \le 250(R_d^3/GM_d)$, and the final density shown in Figure 1 is measured after twice this period. The time step was $0.005(R_d^3/GM_d)$.

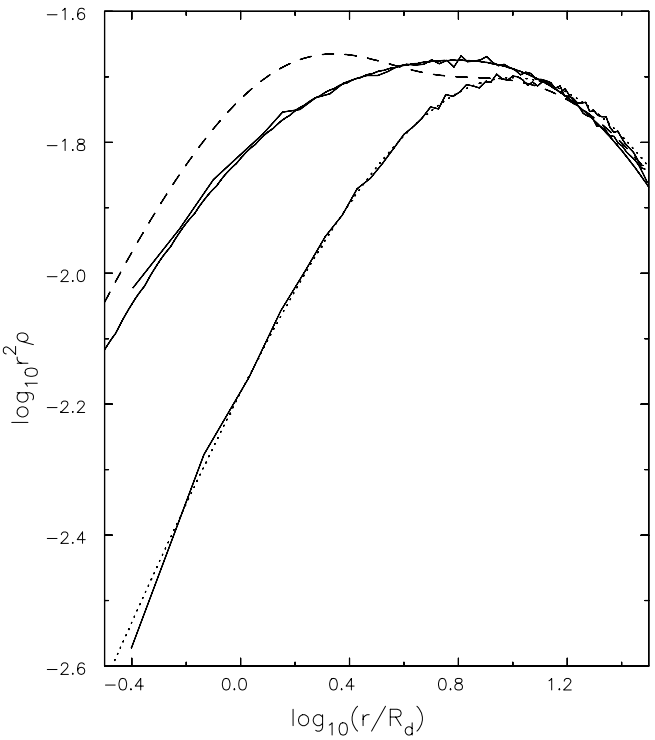

FIG. 1.—Test of the spherical approximation for a disk grown in an NFW halo. The jagged solid lines show the density profile estimated from the particles before and after a thin disk is grown. The dotted and smooth solid lines show the density of the analytic NFW halo and the compressed profile computed from Young's algorithm, respectively. The dashed curve shows the compression predicted by the Blumenthal algorithm, which is clearly inconsistent with the N-body results.

The dotted curve in Figure 1 shows the density function (eq. [6]) that is closely followed by the initial density profile of the 1 million particles (*lower jagged solid line*). The smooth solid line shows the predicted density profile from Young's algorithm after an exponential disk with $l_d = 0.1$ and $m_d = 0.05$ is grown slowly. The upper jagged solid line that follows this curve closely is the (spherically averaged) density profile measured from the particles when the asphericity of the thin disk and halo are taken into account. Evidently, the spherical approximation is quite adequate in Young's algorithm.

The dashed curve in Figure 1 shows the prediction from the Blumenthal algorithm, which is clearly inconsistent with the N-body results. This discrepancy confirms the conclusion reached previously by Barnes (1987), Sellwood (1999), and Gnedin et al. (2004) that the Blumenthal algorithm overestimates halo compression in the inner parts.

A more conventional indication of the difference between the predictions by Young's method and Blumenthal's method is illustrated in Figure 2 for the same model shown in Figure 1. The compressed halo density (Fig. 2, *dot-dashed curves*) predicted by the Blumenthal algorithm is shown on the left, while the right-hand panel shows the prediction from Young's procedure. Note that the greatest differences occur in the inner region where the disk contributes, which is generally the region most strongly constrained by observed rotation curves.

Figure 3 shows the effect of changing the velocity distribution in a Plummer halo model. In all cases shown, the Plummer sphere is compressed adiabatically by the addition of an exponential disk having one-tenth the mass of the halo, and disk scale length of one-tenth of the Plummer core radius. Dejonghe (1987)

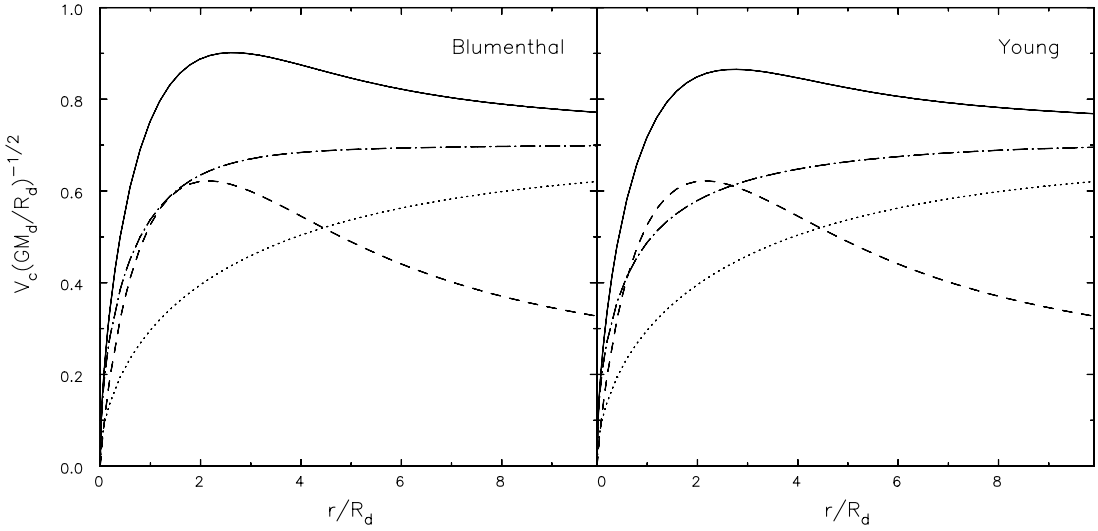

FIG. 2.—Comparison between halo compression using the Blumenthal algorithm (*left*) and Young's formula (*right*), showing that halos are less easily compressed when velocity dispersion is taken into account. In both panels, the solid curve shows the total circular speed, the dashed curve is the disk contribution, the dotted curve is the uncompressed NFW halo, and the dot-dashed curve is the compressed halo contribution. Note that $m_d = 0.05$ in this case.

provides a family of DFs for this model with a single parameter, q, that determines the shape of the velocity distribution. The solid curve in Figure 3 shows the resulting rotation curve when the halo has an isotropic DF ($q = 0$). The dot-dashed curve shows that a DF that is maximally radially biased ($q = 2$) is compressed somewhat less, while the dotted curve shows the result when a strongly azimuthally biased DF ($q = -15$) is assumed. The dashed curve shows the result when the Blumenthal algorithm is employed, again showing that its assumption of extreme azimuthal bias in the orbits of halo particles allows too strong a compression of the halo.

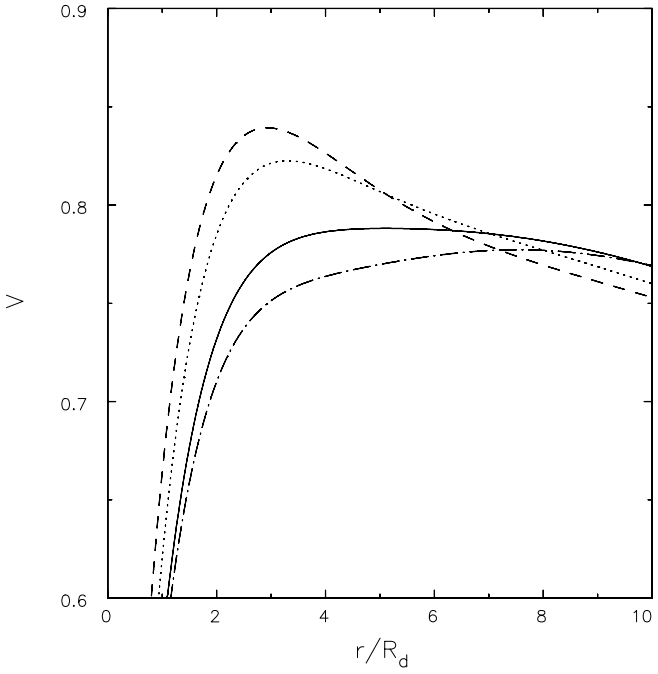

FIG. 3.—Effect of velocity anisotropy in a Plummer halo. The dashed curve shows the circular speed resulting from compression using the Blumenthal algorithm, while the other curves show the same quantity computed by Young's method for different initial DFs. The solid curve is for an isotropic model, the dot-dashed curve is for a model with maximum radial bias, and the dotted curve shows a strongly azimuthally biased model. Note the suppressed zero on the velocity axis: all curves continue approximately linearly to the origin.

The compressed density resulting from Young's method and Blumenthal's method generally shows larger differences for models with cores, such as in King and Plummer models, than for cusped density profiles. However, even for the NFW profile (Fig. 2), the differences remain quite significant.

5. APPLICATION OF YOUNG'S METHOD TO DATA

Here we use Young's algorithm to deduce the initial halos of five galaxies from their observed rotation curves. We present these results here purely to illustrate an application to real data and will report a more systematic study in a later paper.

We selected galaxies with extended H I rotation curves from the compilation of Sanders & McGaugh (2002) so that the shape of the rotation curve is measured well into the halo. In order to explore a range of galaxy properties, we selected five galaxies that span a large range in both luminosity and surface brightness. The five objects are the bright galaxy NGC 2903, the intermediate-luminosity high and low surface brightness galaxies NGC 2403 and UGC 128, and the high and low surface brightness dwarf galaxies NGC 55 and NGC 1560.

We stress that these galaxies were selected to be purely illustrative of our technique over a wide range of galaxy properties and do not constitute a representative sample. They do, however, provide some interesting insights.

We assume an exponential disk, which is adequate for all five galaxies in this very preliminary study, and an NFW halo with an isotropic DF. We have to choose values for our two parameters: the length and mass ratios, l_d and m_d, of the disk and halo. The model halo is dimensionless, so the physical parameters of the primordial halo can be inferred only after scaling to fit a particular galaxy. The conversion to (c, V_{200}) depends weakly on the Hubble constant; we adopt $H_0 = 75$ km s^{-1} Mpc^{-1} for consistency with the galaxy data.

We first constructed a grid of compressed NFW models with a range of plausible m_d and l_d and examined the final rotation curves from this grid to judge which combinations of disk parameters might make tolerable approximations to the data. Crudely speaking, $m_d \leq 0.1$ and $l_d \leq 0.2$ in NFW halos yield plausible-looking

TABLE 1
Disk, Compressed, and Primordial Halo Parameters

Galaxy (1)	V_f (km s^{-1}) (2)	R_d (kpc) (3)	Υ_*[a] (4)	$\mathcal{Q}$ (5)	m_d (6)	l_d (7)	r_s (kpc) (8)	c (9)	V_{200} (km s^{-1}) (10)	References (11)
NGC 2903.....	185	2.0	2.2	0.6	0.10	0.12	16.7	9.2	115	1, 2
NGC 2403.....	134	2.1	0.6	0.4	0.02	0.15	14.0	10.1	106	1, 2, 3
UGC 128.....	131	10[b]	1.1	1.0	0.02	0.19	52.6	3.2	126	4, 5
NGC 55.....	86	2.7[b]	0.2	1.0	0.01	0.10	27.0	4.6	93	6
NGC 1560.....	72	2.6[b]	1.0	1.0	0.01	0.12	21.7	4.9	80	7

[a] In solar units, $M_\odot/L_\odot$, in the B band.
[b] This baryonic scale length is rather larger than that of the stars alone.
References.—(1) Begeman 1987; (2) Wevers et al. 1986; (3) Blais-Ouellette et al. 2004; (4) van der Hulst et al. 1993; (5) de Blok et al. 1995; (6) Puche et al. 1991; (7) Broeils 1992.

rotation curves. A larger m_d compresses the halo too much, leading to rotation curves that have a pronounced peak and fall too far before leveling off. A larger l_d causes the disk to extend too far out into the halo where the declining portion of the rotation curve is too obvious compared to data. This is only an approximate statement: some individual galaxies might be described by more extreme parameters, and different halo types could well require very different combinations of m_d and l_d.

A trend in our grid of models mimics one that is well established by the data. The rotation curves rise quickly and fall gradually for larger values of m_d qualitatively, as observed for luminous spirals. The disk-driven peak declines as we employ a progressively lower m_d, qualitatively giving the gradual, and continuing, rise characteristic of dwarf galaxy rotation curves. Varying l_d at fixed m_d adjusts the amplitude of the total rotation curve relative to that of the baryons.

We used this grid to estimate plausible parameters for a first approximation to the data for each case and then refine the model iteratively. At this juncture, goodness of fit is judged by eye. Our models match the data reasonably well, although they are certainly not perfect. The shortcomings of the fits can in some cases be attributed to deviations from our idealized exponential disk model, which we assume here for simplicity. Indeed, we expect to improve the fits by using the exact disk mass profile, but leave this refinement to future work, as the dominant uncertainty is not in the precise shape of the baryonic mass distribution but in its amplitude, which depends on the stellar mass-to-light ratio Υ_*. For a specific choice of Υ_*, matching both the total and baryonic rotation curves simultaneously restricts the plausible values of m_d and l_d fairly well, although we make no claim that our fits are unique.

We must adopt some estimate for the baryonic mass in each galaxy, which is straightforward for the gas but fraught for stars. McGaugh (2004) discusses the Υ_* for all the galaxies considered here, preferring a prescription that minimizes the scatter both in the baryonic Tully-Fisher relation (McGaugh et al. 2000; McGaugh 2005) and in the mass discrepancy-acceleration relation. He defines the ratio of the adopted Υ_* to this optimal one, as given by the parameter $\mathcal{Q} = \Upsilon_*/\Upsilon_{\rm opt}$, which encapsulates the goodness of the mass-to-light ratio in this respect: the farther $\mathcal{Q}$ is removed from unity, the larger the scatter induced in these otherwise tight correlations.

The basic galaxy data and results are given in Table 1. Column (1) gives each galaxy's name. Column (2) gives the observed flat rotation velocity. Column (3) gives the physical scale length of the exponential disk chosen to approximate each galaxy's baryon profile; since it is the sum of stars and gas that matters, the scale length has been stretched where necessary to approximate the total. Column (4) gives our final adopted mass-to-light ratio Υ_*

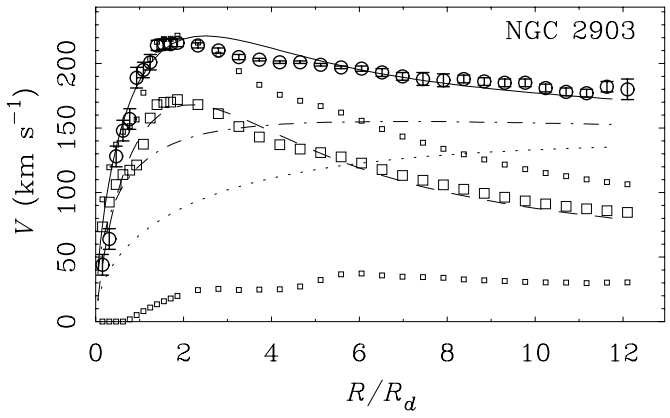

Fig. 4.—Rotation curve and mass model of the luminous high surface brightness galaxy NGC 2903. The rotation curve data are plotted as circles with error bars. The contribution to the rotation by the baryonic component (stars plus gas) is denoted by squares. Large squares are for the modeled mass-to-light ratio specified in Table 1. Also shown as small squares are the limiting cases of the minimum (gas only, with $\Upsilon_* = 0$) and maximum disk. The dashed line shows the adiabatically formed exponential disk used to approximate the observed baryon distribution. The solid line is the total rotation due to disk plus compressed halo. The primordial NFW halo (with parameters given in Table 1) is shown by the dotted line, and the compressed halo is shown by the dot-dashed line.

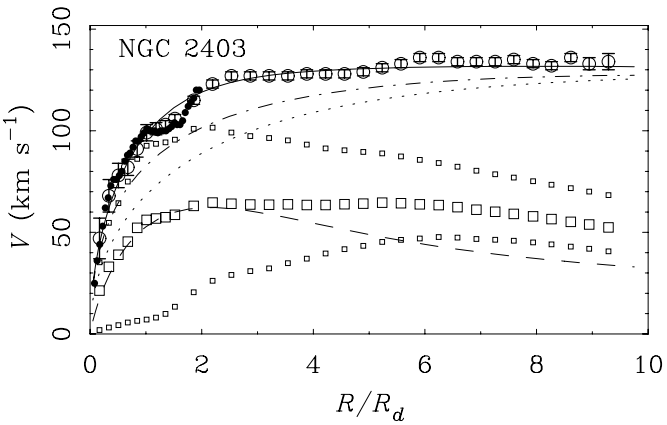

Fig. 5.—Intermediate-luminosity, high surface brightness galaxy NGC 2043. All symbols and lines are the same as in Fig. 4. In addition to the extended H I rotation curve of Begeman (1987), the Fabry-Perot data of Blais-Ouellette et al. (2004) are shown as the small solid points in the rising part of the rotation curve. The extended H I in this galaxy makes it difficult to approximate the baryons with a single exponential disk.

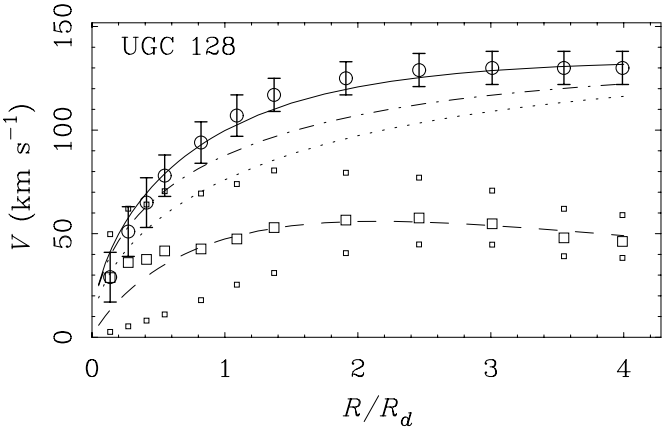

FIG. 6.—Intermediate-luminosity, low surface brightness galaxy UGC 128. All symbols and lines are the same as in Fig. 4. This galaxy is well matched to NGC 2403 in terms of luminosity and circular velocity: these two objects occupy the same location in the Tully-Fisher diagram (de Blok & McGaugh 1996). An approximation to the baryonic component is obtained by stretching the exponential disk scale length to 10 kpc, somewhat longer than that of the stars, which varies from ~6 to 9 kpc, depending on bandpass (de Blok et al. 1995).

(in the *B* band) for the stars. Where possible, this has been held fixed at the optimal value described by McGaugh (2004), but in some cases we had to reduce Υ_* in order to obtain a fit, and we give the deviation from the optimal value in column (5). This deviation is inevitable in the sense that the disk mass must be reduced in order to accommodate the cusp of the NFW halo. Columns (6) and (7) give the halo parameters m_d and l_d of our adopted fit. The scale length of the halo, r_s, corresponding to the baryonic scale length R_d and fitted l_d, is given in column (8). The NFW concentration and V_{200} parameters of the primordial halo are given in columns (9) and (10). References to the original sources of the data used are given in column (11).

The choice of stellar mass-to-light ratio has a pronounced effect on the mass model. There is a tremendous range of possibilities between the maximum and minimum disk (e.g., Fig. 4). Attempts to grow a maximum disk in an NFW halo inevitably lead to rotation curves that peak too high and fall too far before flattening out. For this reason, maximum disks and halos with central cusps appear to be mutually exclusive.

Nevertheless, a heavy disk is important for falling rotation curves. The disk fraction m_d modulates the shapes of rotation curves. Systematic variation of m_d with rotation velocity appears

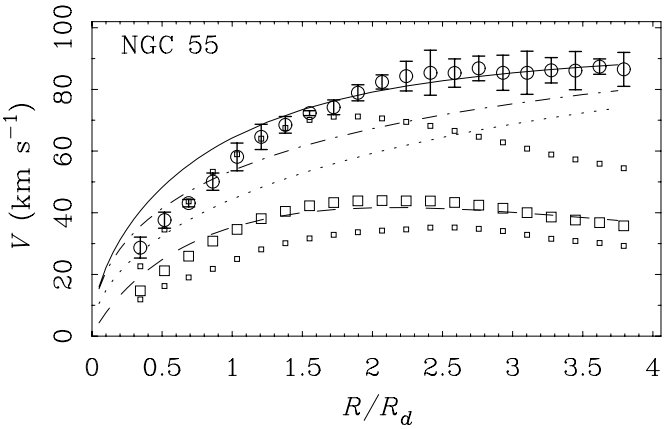

FIG. 7.—High surface brightness dwarf galaxy NGC 55. All symbols and lines are the same as in Fig. 4. The baryonic rotation curve is approximated by an exponential disk of scale length 2.7 kpc (vs. 1.6 kpc for the stars alone).

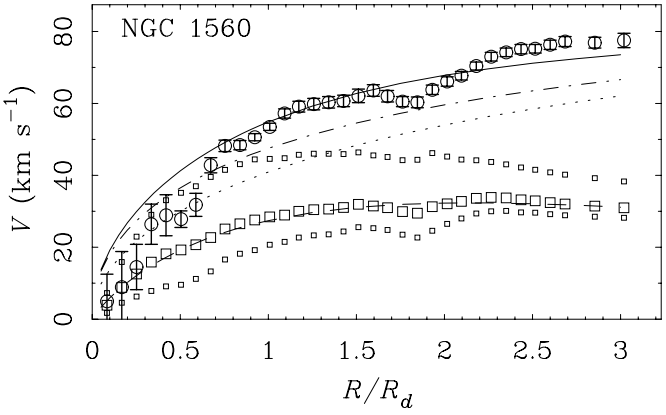

FIG. 8.—Low surface brightness dwarf galaxy NGC 1560. All symbols and lines are the same as in Fig. 4. The baryonic rotation curve is approximated by an exponential disk of scale length 2.6 kpc (vs. 1.3 kpc for the stars alone).

to be required in order to match the observed trend in rotation curve shapes, from falling for bright galaxies to rising for dwarfs (e.g., Persic & Salucci 1991). This variation can be rapid, with $m_d \approx 0.1$ for NGC 2903 falling to $m_d \approx 0.02$ for NGC 2403 (Fig. 5).

Systematic variation of m_d has important ramifications for the Tully-Fisher relation. It implies that the entire observed range of baryonic disks is found in a relatively narrow range of halo masses. Such a finding changes the slope of the Tully-Fisher relation from that nominally predicted for halos only.

UGC 128 (Fig. 6) is comparable to NGC 2403 in luminosity and rotation velocity. Despite the low surface brightness of this galaxy, the halo is perceptibly compressed: the disk is not completely negligible. The disk fraction and l_d are very similar to those of NGC 2403. This is hardly surprising, since the rotation curves of the two galaxies are indistinguishable when normalized by scale length: $V(r)$ is very different, but $V(r/R_d)$ is much the same (de Blok & McGaugh 1996). Consequently, the density of the halo of UGC 128 must be lower than that of NGC 2403, simply because r_s is larger at comparable mass. This is reflected in a low concentration ($c \approx 3$). Although the fit with a compressed NFW halo is good, primordial halo concentrations this low never occur in any plausible cosmology (Navarro et al. 1997; McGaugh et al. 2003).

NGC 55 (Fig. 7) and NGC 1560 (Fig. 8) are nearby dwarf galaxies. The gas is not negligible in these galaxies. The baryonic rotation curve is reasonably well approximated by a single exponential with a scale length stretched relative to that of the stars alone (roughly by a factor of 2) to represent both stars and gas.

In order to produce something like the observed, gradually rising rotation curve, it is necessary to consider very small disk fractions. The cases illustrated with $m_d = 0.01$ provide a good fit to the baryonic components, as well as a reasonable match to the outer parts of the rotation curves. The fit to the inner few kiloparsecs of the rotation curves is not good. The problem here stems from the assumed form of the primordial halo. The NFW halo is too centrally concentrated to begin with, a well-known problem for dwarf galaxies (Côté et al. 2000; de Blok et al. 2001, 2003; Swaters et al. 2003).

6. CONCLUSIONS

We have used the algorithm described by Young (1980), which properly accounts for radial motion, to compute the density of a dark matter halo that is compressed by the growth of a disk in its

center. Young developed the method for compression of a spherical star cluster by growth of a central black hole; the algorithm was applied independently for halo compression by Wilson (2004). While Young's algorithm is more complicated to program, and more time-consuming to run, than the simple and popular algorithm (Blumenthal et al. 1986), it correctly predicts rather less halo compression, especially in the inner region that is most accessible to observations.

The predicted compressed density profiles agree almost perfectly with those found in high-quality *N*-body simulations (Fig. 1) and are significantly less compressed than those predicted by the Blumenthal algorithm. The almost perfect agreement with *N*-body simulations confirms also that the spherical approximation for the disk mass profile is entirely adequate, as previously found by Barnes (1987), Jesseit et al. (2002), and Wilson (2004).

The reason that halos are less easily compressed than predicted by the Blumenthal algorithm is that this crude method neglects the extra pressure caused by radial motions. We present tests (Fig. 3) to show that the compressed density is lowered as the importance of radial motion is increased. Since dark matter halos are formed in a hierarchical collapse, the outer halos are likely to have radially biased velocity distributions, although the inner halos are expected to be close to isotropic.

The algorithm can be applied to all spherical density profiles having valid distribution functions and any arbitrary mass profile for the disk. The key assumptions—that the halo be spherical and that the disk mass was assembled adiabatically—are no more restrictive than those for the usual Blumenthal algorithm. It is expected that hierarchical galaxy formation leads to aspherical dark matter halos, and compression and shape changes can be computed in these more realistic circumstances only by *N*-body simulation (e.g., Kazantzidis et al. 2005).

The adiabatic assumption is likely to hold if the disk remains closely axisymmetric, as the cooling and settling of gas is likely to occur over many crossing times in the inner halo. However, nonadiabatic resonant interactions develop between rotating, nonaxisymmetric structures in the disk and the orbits of halo particles (Tremaine & Weinberg 1984). It is unclear at present whether such interactions can cause significant changes to the halo density profile (Weinberg & Katz 2002; Sellwood 2003).

As proof of principle only, we have derived the parameters of initial, uncompressed NFW halos for a few well-studied galaxies and plan to apply the technique to a larger and more representative sample of galaxies in a later paper. The initial results are promising in many respects. We found it easy to obtain reasonable fits, with variations in disk fraction naturally explaining the variation in shapes of rotation curves. However, it does not appear likely that an improved treatment of halo compression will provide a resolution of the cusp/core controversy, or of the absolute halo density of low surface brightness galaxies, which remains a problem for ΛCDM.

We thank S. Sridhar for drawing our attention to Young's paper, and Greg Wilson and Agris Kalnajs for informing us of their work in advance of publication. The referee, Oleg Gnedin, provided a helpful report. This work was supported by grants AST 05-07323 and NNG 05GC29G to J. A. S. and AST 02-06078 and NAG 513108 to S. S. M.

REFERENCES

Abadi, M. G., Navarro, J. F., Steinmetz, M., & Eke, V. R. 2003, ApJ, 591, 499
Barnes, J. 1987, in Nearly Normal Galaxies, ed. S. A. M. Faber (New York: Springer), 154
Barnes, J., & White, S. D. M. 1984, MNRAS, 211, 753
Begeman, K. G. 1987, Ph.D. thesis, Univ. Groningen
Binney, J., & Tremaine, S. 1987, Galactic Dynamics (Princeton: Princeton Univ. Press) (BT87)
Blais-Ouellette, S., Amram, P., Carignan, C., & Swaters, R. 2004, A&A, 420, 147
Blumenthal, G. R., Faber, S. M., Flores, R., & Primack, J. R. 1986, ApJ, 301, 27
Broeils, A. H. 1992, A&A, 256, 19
Bullock, J. S., Kolatt, T. S., Sigad, Y., Somerville, R. S., Kravtsov, A. V., Klypin, A. A., Primack, J. R., & Dekel, A. 2001, MNRAS, 321, 559
Cohn, H. 1979, ApJ, 234, 1036
Cole, S., Lacey, C. G., Baugh, C. M., & Frenk, C. S. 2000, MNRAS, 319, 168
Côté, S., Carignan, C., & Freeman, K. C. 2000, AJ, 120, 3027
Dalcanton, J., Spergel, D. N., & Summers, J. J. 1997, ApJ, 482, 659
Debattista, V. P., & Sellwood, J. A. 2000, ApJ, 543, 704
de Blok, W. J. G., Bosma, A., & McGaugh, S. S. 2003, MNRAS, 340, 657
de Blok, W. J. G., & McGaugh, S. S. 1996, ApJ, 469, L89
de Blok, W. J. G., McGaugh, S. S., & Rubin, V. C. 2001, AJ, 122, 2396
de Blok, W. J. G., van der Hulst, J. M., & Bothun, G. D. 1995, MNRAS, 274, 235
Dejonghe, H. 1987, MNRAS, 224, 13
Diemand, J., Moore, B., & Stadel, J. 2004, MNRAS, 353, 624
Eggen, O. J., Lynden-Bell, D., & Sandage, A. 1962, ApJ, 136, 748
Fall, S. M., & Efstathiou, G. 1980, MNRAS, 193, 189
Flores, R., Primack, J. R., Blumenthal, G. R., & Faber, S. M. 1993, ApJ, 412, 443
Gnedin, O. Y., Kravtsov, A. V., Klypin, A. A., & Nagai, D. 2004, ApJ, 616, 16
Gottlöber, S., Klypin, A., Kravtsov, A., Hoffman, Y., & Faltenbacher, A. 2003, in High Performance Computing in Science and Engineering, Munich 2002, ed. S. Wagner et al. (Berlin: Springer), 399
Governato, F., et al. 2004, ApJ, 607, 688
Gunn, J. E. 1982, in Astrophysical Cosmology, ed. H. A. Brück, G. V. Coyne, & M. S. Longair (Vatican City: Pontificia Academia Scientiarum), 233
Jesseit, R., Naab, T., & Burkert, A. 2002, ApJ, 571, L89
Jing, Y. 2000, ApJ, 535, 30
Kazantzidis, S., et al. 2005, ApJ, 623, L67
Keeton, C. 2001, ApJ, 561, 46
McGaugh, S. S. 2004, ApJ, 609, 652
———. 2005, ApJ, 632, 859
McGaugh, S. S., Barker, M. K., & de Blok, W. J. G. 2003, ApJ, 584, 566
McGaugh, S. S., Schombert, J. M., Bothun, G. D., & de Blok, W. J. G. 2000, ApJ, 533, L99
McGlynn, T. A. 1984, ApJ, 281, 13
Mo, H. J., Mao, S., & White, S. D. M. 1998, MNRAS, 295, 319
Navarro, J. F., Frenk, C. S., & White, S. D. M. 1997, ApJ, 490, 493
Navarro, J. F., et al. 2004, MNRAS, 349, 1039
Persic, M., & Salucci, P. 1991, ApJ, 368, 60
Puche, D., Carignan, C., & Wainscoat, R. J. 1991, AJ, 101, 447
Ryden, B. S., & Gunn, J. E. 1987, ApJ, 318, 15
Sanders, R. H., & McGaugh, S. S. 2002, ARA&A, 40, 263
Sellwood, J. A. 1999, in ASP Conf. Ser., 182, Galaxy Dynamics, ed. D. Merritt, J. A. Sellwood, & M. Valluri (San Francisco: ASP), 351
———. 2003, ApJ, 587, 638
Spergel, D. N., et al. 2003, ApJS, 148, 175
Swaters, R. A., Madore, B. F., van den Bosch, F. C., & Balcells, M. 2003, ApJ, 583, 732
Tremaine, S., & Weinberg, M. D. 1984, MNRAS, 209, 729
van den Bosch, F. C., & Dalcanton, J. J. 2000, ApJ, 534, 146
van der Hulst, J. M., Skillman, E. D., Smith, T. R., Bothun, G. D., McGaugh, S. S., & de Blok, W. J. G. 1993, AJ, 106, 548
Weinberg, M. D., & Katz, N. 2002, ApJ, 580, 627
Weiner, B. J., Sellwood, J. A., & Williams, T. B. 2001, ApJ, 546, 931
Wevers, B. M. H. R., van der Kruit, P. C., & Allen, R. J. 1986, A&AS, 66, 505
White, S. D. M., & Rees, M. J. 1978, MNRAS, 183, 341
Widrow, L. M. 2000, ApJS, 131, 39
Wilson, G. M. 2004, Ph.D. thesis, Australian National Univ.
Young, P. 1980, ApJ, 242, 1232
Zentner, A. R., & Bullock, J. S. 2002, Phys. Rev. D, 66, 043003